PROCEEDINGS, Twenty-Eighth Workshop on Geothermal Reservoir Engineering
Stanford University, Stanford, California, January 27-29, 2003
SGP-TR-173

MODELING FLUID FLOW AND ELECTRICAL RESISTIVITY IN FRACTURED GEOTHERMAL RESERVOIR ROCKS

Russell L. Detwiler, Jeffery J. Roberts, William Ralph, and Brian P. Bonner

Earth Sciences Division
Lawrence Livermore National Laboratory
7000 East Ave, L-201
Livermore, California, 94551, USA
e-mail: detwiler1@llnl.gov

ABSTRACT

Phase change of pore fluid (boiling/condensing) in rock cores under conditions representative of geothermal reservoirs results in alterations of the electrical resistivity of the samples. In fractured samples, phase change can result in resistivity changes that are more than an order of magnitude greater than those measured in intact samples. These results suggest that electrical resistivity monitoring may provide a useful tool for monitoring the movement of water and steam within fractured geothermal reservoirs. We measured the electrical resistivity of cores of welded tuff containing fractures of various geometries to investigate the resistivity contrast caused by active boiling and to determine the effects of variable fracture dimensions and surface area on water extraction. We then used the Nonisothermal Unsaturated Flow and Transport model (NUFT) (Nitao, 1998) to simulate the propagation of boiling fronts through the samples. The simulated saturation profiles combined with previously reported measurements of resistivity-saturation curves allow us to estimate the evolution of the sample resistivity as the boiling front propagates into the rock matrix. These simulations provide qualitative agreement with experimental measurements suggesting that our modeling approach may be used to estimate resistivity changes induced by boiling in more complex systems.

INTRODUCTION

Evaluating the effectiveness and sustainability of geothermal energy production strategies requires understanding how stresses on the reservoir influence permeability and fluid distribution within the reservoir. The hydraulic response of a reservoir to withdrawal and injection of fluids provides one measure of reservoir performance, but it is difficult to use hydraulic data to infer intra-well details. Electrical techniques such as cross-well EM, electrical resistivity tomography, and the long spacing induction tool (GeoBILT) (Mallan et al., 2002; Wilt et al., 1997) have the potential to complement hydraulic production data by providing quantitative measures of changes in the reservoir between wells. However, these techniques all involve the ability to correlate measurements of electrical resistivity with changes in properties of interest such as fluid saturation.

Electrical resistance is sensitive to properties of both the host rock and the pore fluid (Nesbitt, 1993). Surface conduction, pore-size distribution, and the density of fractures all contribute to reservoir resistivities (e.g. Roberts et al., 2001a; 2001b). In addition, temperature, pressure, chemical composition, and phase distribution of the pore fluid all influence electrical resistance (Brace et al., 1965; Walsh and Brace, 1984). The sensitivity of electrical resistance to such a wide range of variables makes it difficult to predict the electrical response of a geothermal reservoir, but production-induced changes in resistivity can provide valuable insights into the evolution of the host rock and resident fluids. However, understanding the connection between fluid migration due to hydraulic stresses and the resulting electrical response at temperatures and pressures typical of geothermal reservoirs requires controlled experimentation.

We have designed a series of laboratory experiments to evaluate the electrical response of rock cores containing artificial fractures of varying geometries. These experiments provide a unique set of data with which to evaluate our ability to simulate the hydraulic and electrical response exhibited during the experiments. Evaluating and refining computational models for these lab-scale experiments will provide

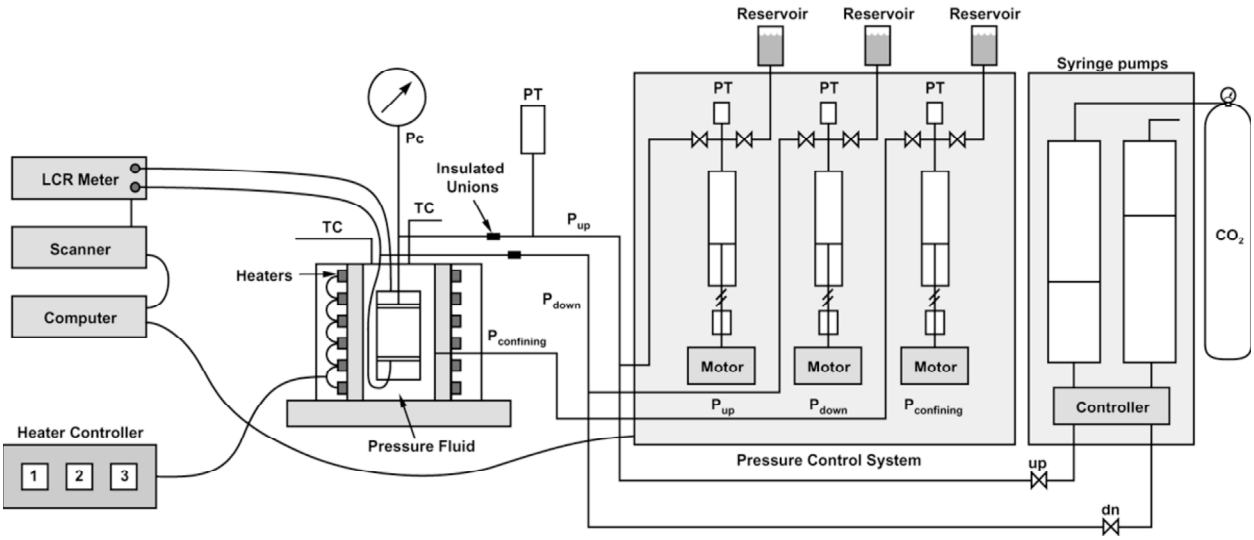

Figure 1. Schematic of the experimental apparatus

insights into which parameters and processes are important when interpreting field-scale electrical data.

EXPERIMENTS

Samples and Preparation

Multiple samples were prepared from the same core of welded tuff. The samples were prepared by machining right-circular cylinders 2.5 cm long and 2.5 cm diameter. A hole drilled along the axis of each sample provided a pathway for flow through the samples. Three samples, TS, TM, and TL, had hole diameters 0.16, 0.42, and 0.65 cm, respectively. While the holes in the samples exhibited different geometry than a fracture, they provided a similar dominant flow path through each sample. The end caps were designed to allow flow to enter and exit the samples only through the holes. Thus, all flow into and out of the rock matrix was radial flow to or from the hole. The ends of each sample were sputter-coated with gold to ensure good electrical connection between the rock and the end caps. Porosity was determined by subtracting dry density from wet density. Dried and evacuated samples were immersed in a solution of high-purity NaCl and degassed, distilled water (1.65 g/l NaCl). Fluid resistivity at room temperature was ~6.4 Ω-m (conductivity = 1.53 mS/cm).

Experimental apparatus

The apparatus consists of an externally heated pressure vessel with separate pumps and controls for confining pressure and pore pressure on either side of the sample (Figure 1). Roberts et al. (2001a) provide a complete description of the experimental apparatus and measuring procedures. Pore pressure was controlled independently between 0 and 3.6 MPa with two syringe pumps capable of accurately controlling pressure or volume. For convenience the two pumps are referred to as up- and down-stream pressure systems. An impedance bridge was used to measure the resistance of the electrically isolated samples at 1 kHz. Electrical resistivity was calculated from the resistance and geometry of the core. Temperature was measured with two type T thermocouples with an accuracy of ±2°C. One thermocouple was placed in the confining fluid near the sample and the other protruded through the end cap partway into the hole in the sample to measure the transient response of the pore fluid temperature during phase changes. Resistivity measurements have been made at temperatures up to 275 C. Data collection was automated using a scanning unit and microcomputer.

Experimental procedures

After placing each sample in the pressure vessel, the pore and confining pressures were raised to 1.15 and 3.59 MPa, respectively. The temperature of the samples was controlled at 166 C. At this temperature and pressure, the transition from liquid to vapor occurs at 0.72 MPa.

Three different experiments were conducted on each of the cores: 1) a constant pressure test, 2) a shut-in test, and 3) a drawdown test. Each of these tests imposed different hydraulic boundary conditions on

the sample resulting in different electrical response during each test. The constant pressure test involved instantaneously lowering the pore pressure to 0.46 MPa and controlling the pore pressure at this pressure for the duration of the experiment. The shut-in test was initiated by instantaneously lowering the pore pressure to 0.46 MPa, controlling the pressure for 30 seconds and then isolating the sample from the pressure control system. A pressure transducer measured the subsequent rise in pressure caused by fluid migrating from the rock matrix towards the hole. During the drawdown test, a constant volumetric flow rate of 0.003 ml/min was withdrawn from the sample causing the pore pressure to gradually reduce.

Experimental results

Because it is the changes in electrical resistivity that reflect migration of fluids within the samples, we converted the measured electrical resistance to normalized resistivity, ρ/ρ_o, where ρ_o is the initial, saturated resistivity of each sample.

Figure 2 shows ρ/ρ_o plotted against time for each of the constant pressure tests. Immediately after lowering the pressure in each sample, ρ/ρ_o increases due to the transition of the liquid in the hole to steam. The magnitude of the jump in ρ/ρ_o reflects the size of each hole. The transition of the liquid in the hole to vapor also causes a decrease in temperature of ~20 to 30 C, however, due to the frequency of data collection (4 / min.), and the relatively rapid decrease and subsequent rise in temperature, the thermocouple readings did not always coincide with the low temperature in the hole. The thermocouple measurements confirm that the temperature in the holes returns to equilibrium (166 C) much more quickly than the pressures and resistivities reach steady state for any of these tests.

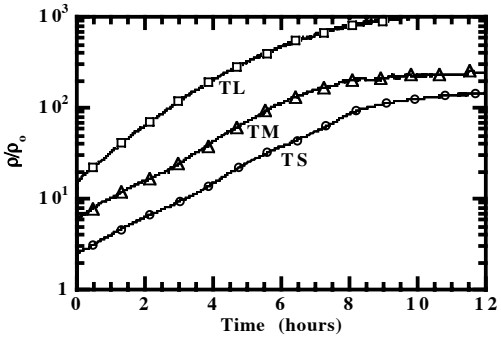

Figure 2. Normalized resistivity plotted versus time for the constant pressure tests.

After the initial increase, ρ/ρ_o gradually increases as the boiling front induced by the reduced pressure in the hole propagates into the matrix. For each of the samples, ρ/ρ_o exhibits a log-linear increase until the phase distribution within the sample nears equilibrium, at which point the rate of change in ρ/ρ_o begins to decrease.

Figures 3 shows ρ/ρ_o and P/P_{boil} (where P is the pressure in the hole and P_{boil} is the phase transition pressure at 166 C) plotted against time for the shut-in tests in samples TS and TL. As with the constant pressure tests, when the pressure is dropped at the start of the test, the liquid in the hole changes to steam, and the resistivity rises. However, because the sample is isolated from the pressure control system after 30 seconds, fluid migrating from the rock into the hole causes the pressure in the hole to rise. The

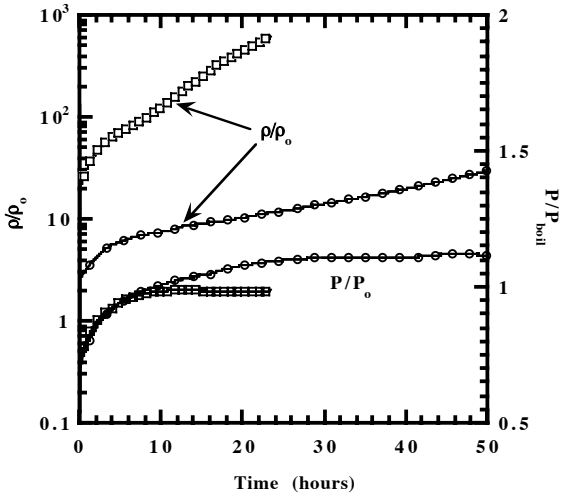

Figure 3. Normalized resistivity and pressure plotted versus time for the shut-in tests in sample TS (circles) and TL (squares).

pressure in the large-hole sample (TL) appears to reach steady state more quickly than for the small hole. However, the continued increase in ρ/ρ_o suggests that the distribution of liquid and vapor in the pore space of the rock matrix has not fully equilibrated. Furthermore, in TS, fluid migrating from the rock matrix into the hole caused the pressure to rise above P_{boil}, whereas in TL, the pressure leveled off at P_{boil}. This indicates that in TS, the fluid in the hole condensed due to flow from the matrix, but in TL remained as vapor.

Figures 4a and 4b show P/P_{boil} and ρ/ρ_o, respectively, plotted against dimensionless time, t' = tQ/V, where t is time, Q is the volumetric flow rate from the sample, and V is the volume of the hole. For each

test, t' was set to zero at the time the pressure in the hole reached P_{boil} to facilitate direct comparison of the experiments. For a non-porous rock matrix and a hole filled with an ideal gas, the steady volumetric extraction of fluid from the hole would result in similar reductions in pressure with t'. This suggests that the different responses of P/P_{boil} exhibited in Figure 4a for each sample result from the different

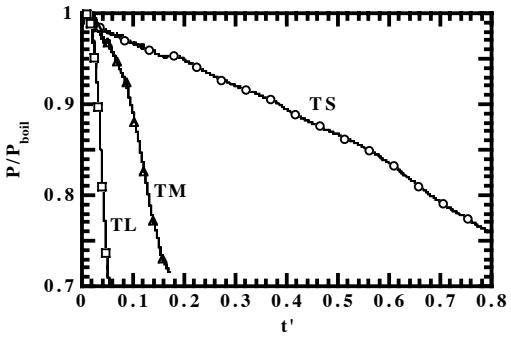

Figure 5a. Normalized pressure plotted versus t' for the drawdown tests.

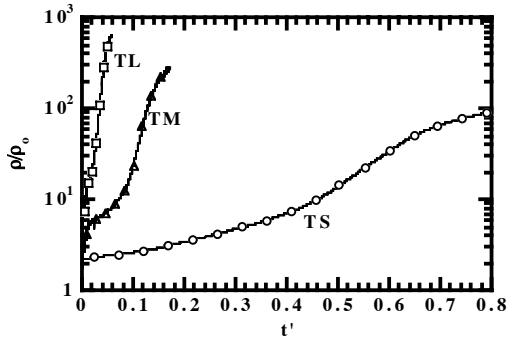

Figure 4b. Normalized resistivity plotted versus t' for the drawdown tests.

rates of fluid flow from the rock matrix in response to pumping from the hole. Thus, for sample TS, though the hole in the sample has a smaller diameter than the hole in sample TL, the relative rate of drawdown in the hole is slower in sample TS. This is reflected in the measurements of ρ/ρ_o, which demonstrate that a two order of magnitude increase in ρ/ρ_o occurs at t'~0.04 in sample TL and t'~0.8 in sample TS.

COMPUTATIONAL MODELING

The series of experiments described in the previous section provide an excellent data set with which to test our ability to model fluid migration in geothermal rocks under controlled conditions. Our modeling efforts employed the Nonisothermal Unsaturated Flow and Transport model (NUFT) developed by Nitao (1998). We used NUFT to solve the continuum-scale mass and energy balances for the liquid and vapor phases and simulate flow and the evolving phase distribution within the rock matrix. Our preliminary results focus on the constant pressure tests presented in Figure 2. Parameters used to describe the mass and heat transport properties of the rock matrix were independently measured for cores from the same layer within the same formation as the samples used for the current experiments. The hole was assigned separate material properties selected to represent an empty hole. The values of parameters used for the simulations are summarized in Table 1.

Table 1: Summary of model parameters

Parameter	Rock matrix	Hole
K – permeability (m^2)	7.2e-18	1.0e-6
ϕ - porosity	0.157	1.0
c_p - specific heat (J/kg C)	1040	N/A
ρ_b (kg/m^3)	2513	N/A
Thermal conductivity (W-m/ C)		
solid	1.74	N/A
liquid	2.34	2.34
gas	1.74	1.74
S_r - residual saturation	0.07	1.0e-5
m - van Genuchten param.	0.29	0.5
α - van Genuchten param.	1.14e-5	.00114
Δr – grid spacing (m)	2.0e-4	2.0e-4

Figure 5 shows simulated saturation profiles for samples TL and TS at a sequence of times. The liquid saturation decreases as the pressure drop propagates into the rock matrix and steam flows towards the hole. As expected, the time-scale required to reach a steady-state saturation distribution is longer for the sample with the smaller hole (TS) due to a smaller surface area between the hole and the rock matrix.

Previous experimental efforts to quantify the relationship between liquid saturation, S, and ρ have yielded a model of $\rho(S)$ (Roberts, 2001) at temperatures up to 95 C. They used an Arrhenius relationship

$$\sigma = \sigma_o \exp(-Ea/kT) \qquad (1)$$

to quantify conductiviy ($\sigma = 1/\rho$), where Ea is the activation energy, k is the Boltzmann constant, T is the temperature. This relationship was found to represent σ well for S greater than ~0.15 - 0.2. Subsequently, Roberts et al. (2001b) extended this relationship to temperatures above 100 C to estimate electrical resistivities in a field-scale experiment. We use this relationship to estimate the electrical resistivities from simulated saturation profiles such as those presented in Figure 5.

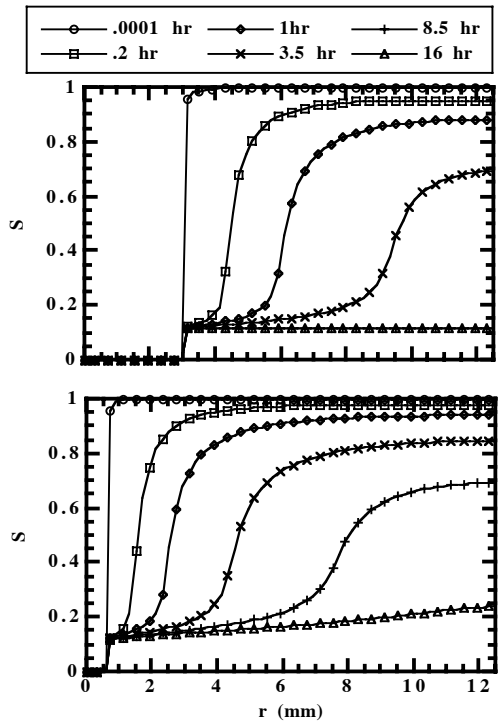

Figure 5. Simulated saturation profiles at equal times in TL (upper plot) and TS (lower plot) during constant pressure simulations.

Figure 6 shows simulated values of ρ/ρ_o for samples TS and TL. The simulations exhibit good qualitative agreement with the experimental results presented in Figure 2. The initial increase in ρ/ρ_o caused by boiling the fluid in the hole at t~0 is similar for both samples and the near steady-state value of ρ/ρ_o is closely approximated for sample TL, but for sample TS, the simulation underestimates the final value of ρ/ρ_o by ~1/2 order of magnitude. In addition, the time-scales required to near steady state are similar for the experiments and simulations. There are several notable differences between the experiments and simulations. The simulations transition more quickly from increasing ρ/ρ_o to a steady value that the experiments. This is likely due to pore-scale redistribution of the fluid in the rock matrix than can result in measurable changes in ρ, especially at low saturations, but cannot be easily included in a continuum-scale model. Also, the shape of the curve between t=0 and steady state is different for the simulations. Ongoing sensitivity analysis of the computational model to material properties and model parameters may help to illuminate the cause of this discrepancy. These sensitivity studies will also help to clarify the relative importance of different parameters when trying to interpret field-scale measurements of electrical resistivity.

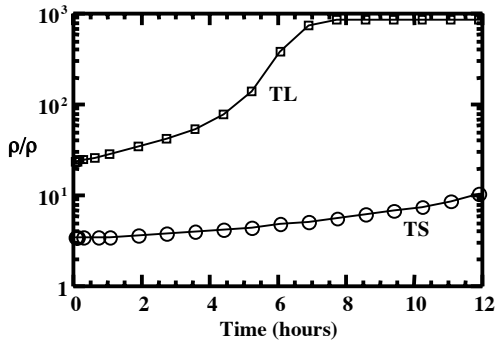

Figure 6. Normalized resistivity plotted versus time for the constant pressure simulations.

SUMMARY

The ability to infer hydraulic behavior from electrical measurements in the field is based upon the relationship between electrical resistance and properties such as saturation, temperature, and pressure. Understanding the interaction of these variables and their influence on numerical simulations at the laboratory scale is fundamental to interpreting larger scale field data. We have presented results from a systematic series of laboratory experiments specifically designed to test our ability to simulate flow, phase distribution, and electrical response under conditions typical of geothermal reservoirs. Preliminary modeling results demonstrate reasonable qualitative agreement with the experimental results. More extensive simulations over the full range of experimental boundary conditions should help to clarify sources of discrepancies between experiments and simulations. Additionally, sensitivity studies in which model parameters are systematically varied will shed light on the relative importance of the many parameters involved in modeling two-phase flow in geothermal systems and their role in estimating changes in electrical resistivity.

ACKNOWLEDGMENTS

This work was performed under the auspices of the U. S. Department of Energy by the University of California, Lawrence Livermore National Laboratory under Contract No. W-7405-Eng-48.

REFERENCES

Brace, W. F., Orange, A. S., and Madden, T. R. (1965), The effect of pressure on the electrical resistivity of water-saturated crystalline rocks, *Journal of Geophysical Research*, **70**, 5669-5678.

Llera, F. J., Sato, M., Nakatsuka, K., and Yokoyama, H. (1990), "Temperature Dependence of the

Electrical Resistivity of Water-Saturated Rocks," *Geophysics,* **55,** 576–585.

Mallan, R, Wilt, M, Kirkendall, B, Kasameyer, P. (2002), 3D Extended Logging for Geothermal Resources: Field Trials with the Geo-Bilt System, *Geothermal Resources Council, Transactions, 26,* 405-410.

Murray, L. E., Rohrs, D. T., Rossknect, T. G., Aryawijawa, R., and Pudyastuti, K. (1995), "Resource Evaluation and Development Strategy, Awibengkok Field," Proceedings World Geothermal Congress, Florence, Italy, pp. 1525–1531.

Nitao, J.J.. Reference manual for the NUFT flow and transport code, Lawrence Livermore National Laboratory, UCRL-MA-130651, 1998.

Nesbitt, B. E. (1993), Electrical Resistivities of crustal fluids, *Journal of Geophysical Research,* **98,** 4301-4310.

Roberts, J. J. (2001), Electrical properties of microporous rock as a function of saturation and temperature, *Journal of Applied Physics*, *21*, 1687-1694.

Roberts, J. J., Bonner, B. P., and Duba, A. G. (2000), "Electrical Resistivity Measurements of Andesite and Hydrothermal Breccia from the Awibengkok Geothermal Field, Indonesia," *TwentyFifth Annual Stanford Geothermal Reservoir Engineering Workshop*, 339-344.

Roberts, J. J., Duba, A. G., Bonner, B. P., and Kasameyer, P. (2001a), "Resistivity During Boiling in the SB-15-D Core from The Geysers Geothermal Field: The Effects of Capillarity," *Geothermics, 30*, 235-254.

Roberts, J. J., A. Ramirez, S. Carlson, W. Ralph, W. Daily, and B. P. Bonner (2001b), Laboratory and field measurements of electrical resistivity to determine saturation and detect fractures in a heated rock mass, *Geothermal Resources Council, Transactions, 25,* 681-686.

Walsh, J. B., and Brace, W. F. (1984), The effect of pressure on porosity and the transport properties of rock, *Journal of Geophysical Research,* **89,** 9425-9431.

Wilt, M., Takasugi, S., Uchida, T., Kasameyer, P., and Lee, K. H. (1997), Fracture mapping in geothermal fields with long-offset induction logging, *Proceedings, Twenty-Second Annual Stanford Geothermal Reservoir Engineering Workshop*, 229-232.